SUPPLEMENTARY INFORMATION

Enhanced sensitivity in nonlinear parity-time symmetric silicon micromechanical resonators

Yu-Jue Xie, Li-Feng Wang*, Man-Na Zhang, Rui Wang, and Qing-An Huang*

Key Laboratory of MEMS of the Ministry of Education, Southeast University, Nanjing 210096, China.
*e-mail: wanglifeng@seu.edu.cn; hqa@seu.edu.cn

Contents

S1. Simulations of PT-symmetric silicon micromechanical resonators

The application of the mechanical-electric analogy is prevalent in Micro-Electro-Mechanical Systems (MEMS), where an equivalent circuit can be used to represent two coupled micromechanical resonators[1]. Fig. S1a depicts this equivalent circuit for the aforementioned resonators. The correlation between parameters in the mechanical and electrical systems can be described by the equations $R_i = c_i/\eta^2$, $L = m/\eta^2$ and $C_i = \eta^2/k_i$. In this study, we have extracted the conversion coefficient η^2 as 7.4773×10^{-15}. The converted loss resistance, denoted as R_l, was found to be 195.56 MΩ—a value too large for implementation using a nonlinear resistor. Consequently, we applied a proportional scaling to the conversion coefficient, represented as $\eta'^2 = \eta^2 \times 10^8$, which is equivalent to 7.4773×10^{-7}. It is important to note that this scaling does not alter key parameters such as the resonance frequency. We conducted transient simulations of the coupling circuit using ADS software, with the circuit currents representing the sensing current. These currents were then converted to output voltage through a TIA. Fig. S1b provides a schematic diagram of this process along with the detailed ADS configuration. Table S1 contains all parameters extracted from measurements, with the electrical parameter calculated based on η'^2. The negative resistance, substituted by the amplifier, can provide an equivalent negative resistance to that of the loss port, as shown in Fig. S3c. The simulations were conducted following the experimental parameter settings provided in Fig. S3d. Simulation results indicate that the system maintains steady-state oscillation at a specific frequency, reaching a new steady-state oscillation within a fraction of a second after applying a perturbation.

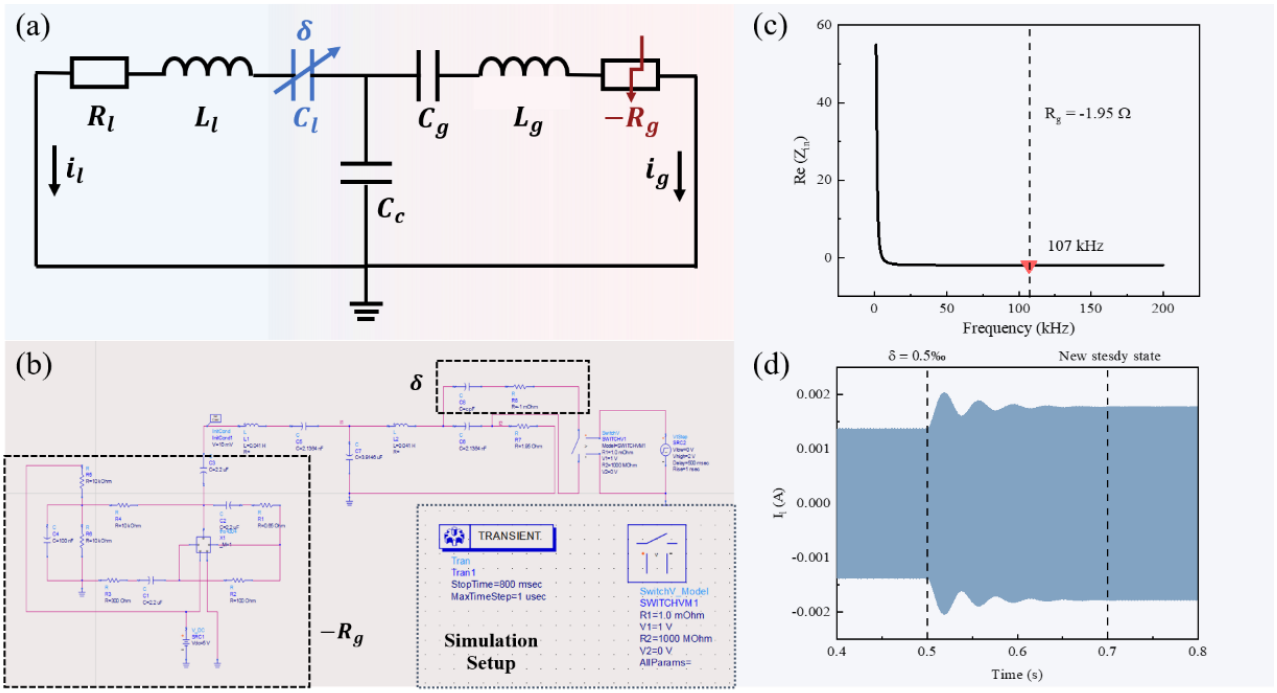

Supplementary Fig. 1. Simulations of time-domain signals. (a) Equivalent RLC circuit schematic diagram for two coupled micromechanical resonators, (b) ADS schematic diagram and setting, (c) The negative resistance formed by the amplifier, and (d) Time-domain response of node voltages on the gain resonator when a perturbation is applied on the loss resonator.

Supplementary Table 1. Parameters used for simulations

Mechanical parameter		Electrical parameter	
m(kg)	$3.0653' 10^{-8}$	L(H)	0.0410
c_l(N×s/m)	$1.4623' 10^{-6}$	R_1(Ω)	1.9556
k_c(N/m)	0.1910	C_c(μF)	3.9146
k(N/m)	350	C(nF)	2.1364

S2. Nonlinear gain

The feedback loop in the AGC provides the nonlinear gain, which is adequately fitted by

$$A_G = \frac{B}{1 + \left(\frac{v_{in}}{V_G}\right)^{\beta}}, \tag{S1}$$

where v_{in} is the input voltage, V is the gradual saturation voltage, A is the gain under low voltage limit, and β is the index describing the nonlinearity. The gain curve of the AGC is obtained by testing the variation of its output voltage with respect to the input voltage, where the gain is defined as the ratio of output to input. The results are shown in Fig. S2a. Experimental curve indicates that the gain is linear for small input voltages and gradually transitions into a nonlinear region as the input voltage increases, providing saturated gain. Fitting the curve yields the parameters $B = 47.59$, $V_G = 0.0087$ V, and $\beta = 4$.

The nonlinear gain of the AGC is influenced by the magnitude and direction of the applied perturbations, and the impact of $\pm\delta$ is reflected in the input voltage V_{in}, which is the output voltage of the gain resonator V_g. The amplitudes of the gain resonator under different perturbations are measured and substituted into Eq. (S1) to calculate the corresponding AGC gain. The results are presented in Fig. S2b. The results show that under perturbations in different directions $\pm\delta$, the gain consistently changes in the same direction, providing varying gains under different perturbations to meet the requirements for stable oscillation.

where v_{in} represents the input voltage, V_G denotes the gradual saturation voltage, B signifies the gain under low voltage levels, and β characterizes the nonlinearity index. The gain curve for the Automatic Gain Control (AGC) is derived by examining the correlation between the output and input voltages, with the gain defined as their ratio. As illustrated in Fig. S2a, experimental data suggests that the gain exhibits linearity for smaller input voltage levels, transitioning into a nonlinear region as input voltage levels increase, resulting in a saturated gain. Curve fitting yields parameters $B = 47.59$, $V_G = 0.0087$ V, and $\beta = 4$.

The nonlinear gain of the AGC is influenced by both the magnitude and direction of applied perturbations, with the impact of $\pm\delta$ reflected in the input voltage v_{in}, which is the output voltage (V_g) on the gain resonator. By measuring the voltage amplitudes of the gain resonator under various perturbations and substituting these values into Eq. (S1), the corresponding AGC gain is calculated. These findings are depicted in Fig. S2b, indicating that with perturbations in different directions ($\pm\delta$), the gain consistently varies in the same direction, thus accommodating diverse gains under different perturbations to ensure stable oscillation.

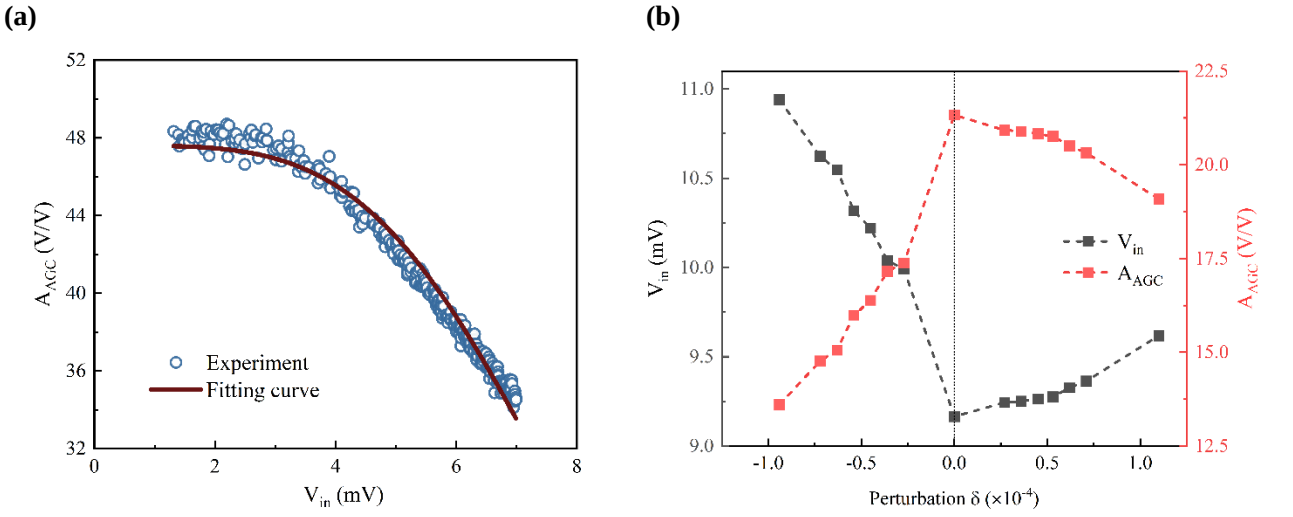

Supplementary Fig. 2. (a) The measured nonlinear gain of the AGC as a function of input voltage. (b) Measured input voltage amplitude in AGC and the corresponding gain as a function of perturbation.

S3. Fabrication process flow

The fabrication process flow is illustrated in Fig. S3. Firstly, the silicon micromechanical resonators were fabricated using a Silicon on Insulator (SOI) wafer, comprising a 400 μm substrate, a 2 μm oxide layer, and a 25 μm structural layer. A layer of negative photoresist was then applied to the wafer, patterned, and exposed using a first-level mask via lithography. Subsequently, Ti/Au metal electrodes were formed by depositing onto the photoresist, followed by a lift-off process. A UV-sensitive photoresist layer was then coated, patterned using a second-level mask, and developed to expose the device layer. The silicon was etched down to the oxide layer using SF_6 and C_4F_8 gases, ensuring vertical sidewalls. Finally, the photoresist was stripped with an organic solvent and oxygen plasma, followed by HF wet etching to remove the oxide layer and release the suspended silicon micromechanical structure.

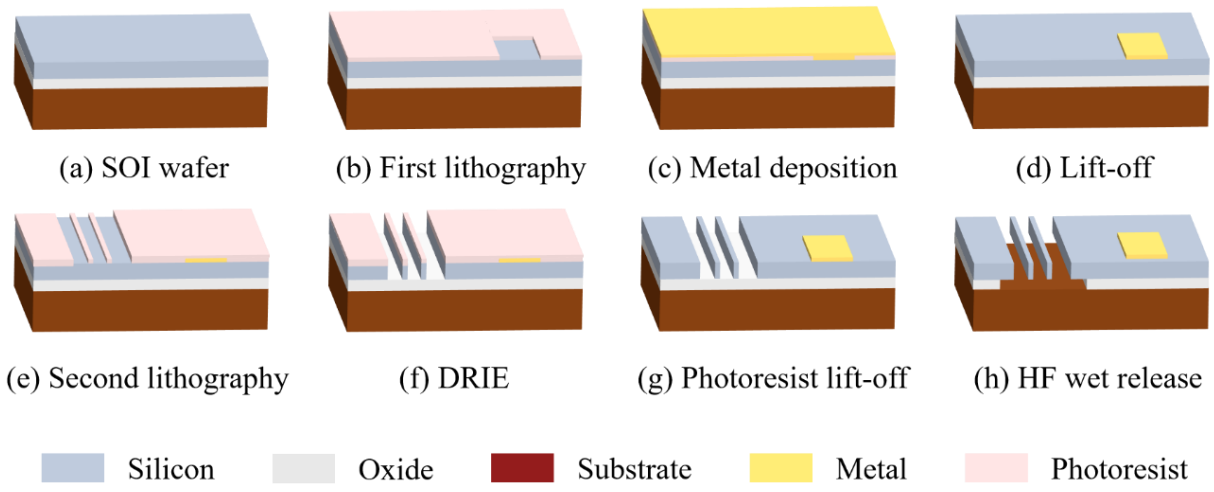

Supplementary Fig. 3. The fabrication process flow for silicon micromechanical resonators.

S4. Experimental setup

The illustration of all instruments and their interconnections is presented in Fig. S4.

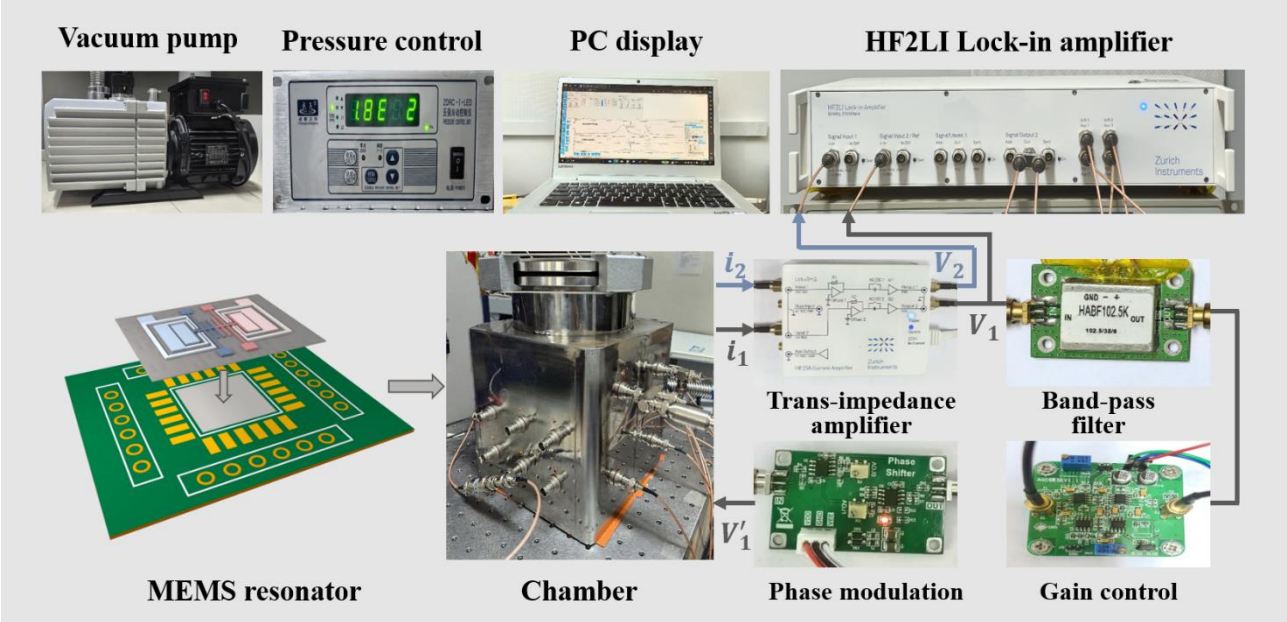

Supplementary Fig. 4. Experimental setup of PT-symmetric silicon micromechanical systems.

Reference

1. Tilmans, H. Equivalent circuit representation of electromechanical transducers: I. Lumped-parameter systems. *J. Micromech. Microeng.* **6**, 157-176 (1996).